Sphingomyelin is critical in organizing phosphoinositide dynamics during phagocytic uptake of *Mycobacterium tuberculosis*

Patrick Niekamp, Gaelen Guzman, Hans Leier, Ali Rashidfarrokhi, Veronica Richina, Joost Holthius, Fikadu G. Tafesse[1]

[1]Department of Molecular Microbiology & Immunology, Oregon Health & Science University (OHSU), Portland, OR 97239, USA

[*]Correspondence: tafesse@ohsu.edu

Abstract

Tuberculosis, the pathological result of infection by *Mycobacterium tuberculosis* (*M.tb*), represents a massive and persistent global health burden with vast overrepresentation in regions with poor access to healthcare. This pathogen survives intracellularly within lung macrophages, and has been shown to extensively reprogram the host lipid compartment to the effect of enhanced survival and immune evasion. Sphingolipids are a class of lipid with extensive functions in a wide variety of cellular contexts, including apoptosis, autophagy, stress response, and inflammation. There remains a significant knowledge gap surrounding the lipid-mediated interactions between *M.tb* and its host. Our investigation aims to explore the mechanisms through which *M.tb* harnesses host-derived sphingolipids to gain entry to the host and to survive intracellularly. To this end, we use chemical and genetic perturbations of the sphingolipid *de novo* synthesis pathway and fluorescence microscopy to show that sphingolipids are required for efficient phagocytosis of *M.tb*. We furthermore show that the dynamics of phosphoinositides at the phagosomal synapse are perturbed upon blockade of sphingolipid synthesis. Finally, we demonstrate that perturbing the homeostasis of a specific sphingolipid (sphingomyelin) through both enrichment

and depletion at the cell surface reduces *M.tb* uptake. This work represents a first step in building comprehensive knowledge of the mechanisms of host-pathogen interactions in *M.tb*, and demonstrates a cohort of methodologies that may be applied to a variety of pathogenic contexts.

Introduction

Phagocytosis is critical for clearing dead and effete cells, and serves as a first line of defense against pathogens such as bacteria, parasites, and fungi. Phagocytosis culminates in the engulfment and internalization of target particles, which are subsequently degraded via passage through the endocytic pathway. This cellular process is distinct from other forms of extracellular uptake, including endocytosis and micropinocytosis, in that phagocytosis is necessarily initiated by the engagement of receptor to multi-valent ligand on particles >0.5um in diameter (Levin, Grinstein, & Schlam, 2015). While all eukaryotic cells are capable of phagocytic uptake, the bulk of phagocytosis in mammals is performed by professional phagocytes with a common myeloid precursor: monocytes, macrophages, dendritic cells, neutrophils, and mast cells (Stuart & Ezekowitz, 2005). In the context of pathogenic clearance, phagocytosis results in robust inflammatory response and presentation of antigen to the adaptive immune response (Levin et al., 2015).

Some pathogens, however, thrive within the phagosomal compartment – of particular note is *Mycobacterium tuberculosis* (*M.tb*). This bacterium is the etiologic agent of tuberculosis, an ancient and devastating disease. This pathogen is referenced in the earliest records of human history, and currently remains a massive global health burden – in 2018, *M.tb* was responsible for an estimated 1.3 million deaths among HIV-negative individuals, and an additional 300,000 deaths among HIV-positive individuals (Daniel, 2006; *Global*

49 *tuberculosis report 2018.*, 2018). A highly-specialized intracellular pathogen, *M.tb* en-
50 gages phagocytic receptors on alveolar macrophages and dendritic cells to establish in-
51 fection. It thensubverts host immune responses to evade lysosomal degradation and rep-
52 licate within a modified phagosomal compartment (Cambier, Falkow, & Ramakrishnan,
53 2014).

54 As *M.tb* must interact with host membranes and lipids at nearly all stages of its infec-
55 tive lifecycle, it is critical to develop an understanding of the specific mechanisms of host-
56 pathogen interactions at the lipid level. Research suggests that *M.tb* induces substantial
57 lipidomic reprogramming in its host. Notably, this pathogen has been shown to interfere
58 with Ca^{2+}-induced phagosomal maturation by interfering with the activity of sphingosine
59 kinase, which produces the potent signaling molecule sphingosine-1-phosphate (Malik et
60 al., 2003; Thompson et al., 2005). However, the specific functional roles played by host
61 lipid species at the site of phagocytic uptake of *M.tb* have remained relatively unstudied.
62 In particular, the structural and signaling functions played by sphingolipids at the cell
63 membrane and within the phagosome during *M.tb* infection are virtually unknown.

64 Sphingolipids are a complex family of natural lipids that contain a sphingoid base.
65 Recent research has shown that sphingolipids mediate functions beyond membrane bar-
66 rier components; these lipids accumulate in lipid rafts and act as secondary messengers
67 within the cell (El Alwani, Wu, Obeid, & Hannun, 2006; Hla & Dannenberg, 2012; Taha,
68 Mullen, & Obeid, 2006). These functions are relevant to many disparate biological pro-
69 cesses that span from apoptosis and autophagy to stress response and inflammation
70 (Hakomori & Igarashi, 1995; Hannun & Obeid, 2002; Snider, Alexa Orr Gandy, & Obeid,
71 2010). Of particular interest to the study of phagocytosis, sphingomyelin is enriched to

72 the exoplasmic leaflet, and has been shown to contribute to the formation of cholesterol-
73 enriched lipid rafts – its synthesis is mediated by sphingomyelin synthase-1 in the Golgi
74 network and sphingomyelin synthase-2 in lysosomes, and it is degraded at the cell mem-
75 brane by sphingomyelinase (García-Arribas, Alonso, & Goñi, 2016; Hla & Dannenberg,
76 2012; van Meer & de Kroon, 2011). Additionally, sphingosine 1-phosphate (S1P), pro-
77 duced by sphingosine kinase, acts through various S1P receptors to activate a wide range
78 of signaling processes; these S1PRs have been shown to activate several factors related
79 to phagocytosis, including Rac, phospholipase C, and PI_3K (Snider et al., 2010). As such,
80 this investigation endeavors to elucidate the roles played by this dynamic lipid class in the
81 phagocytic uptake of *M.tb*.

82 To determine the functions of sphingolipids in phagocytosis, we chemically and ge-
83 netically manipulated various stages of the sphingolipid metabolic pathway in multiple
84 lines of immunologically-relevant phagocytes of murine and human origin (macrophages,
85 dendritic cells, and monocyte-derived macrophages), performed uptake assays with the
86 intracellular pathogen *M.tb*, and visualized the progression of phagocytosis using fluores-
87 cence microscopy. We first demonstrate that the efficiency of phagocytic uptake of *M.tb*
88 is significantly impaired when bulk sphingolipid synthesis is inhibited in murine and human
89 host cells. In characterizing this observation, we show that the initial stages of phagocy-
90 tosis (particle binding and recognition) are largely unaffected by defects in sphingolipid
91 synthesis, but that sphingolipid-deficient cells are defective in the propagation of phago-
92 cytic signaling beginning at intermediate stages of phagocytosis (engulfment, and inter-
93 nalization). We observe that cell devoid of sphingolipids fail to convert phosphatidylinosi-
94 tol 4,5-*bi*sphosphate to phosphatidylinositol 3,4,5-*tris*phosphate – producing an overall

95 defect in proper phagosome formation. Next, we show that genetically blocking the syn-
96 thesis of sphingomyelin at the cell membrane confers a defect in the phagocytic uptake
97 of *M.tb*. These findings highlight the diversity of functions that sphingolipids play during
98 this immunologically significant phase of the *Mycobacterium tuberculosis* infectious lifecy-
99 cle.

100 **Results**

101 *Chemical inhibition and genomic editing effectively blocks sphingolipid synthesis in phag-*
102 *ocytes*

103 Cellular proportions of sphingolipids are maintained primarily through a central *de*
104 *novo* synthesis pathway and secondarily through salvage pathways. The rate-limiting first
105 step of sphingolipid synthesis is mediated by the serine palmitoyltransferase (SPT) com-
106 plex in the ER to produce the sphingoid base from serine and palmitoyl-CoA. Just down-
107 stream, ceramide is produced by ceramide synthase (CerS). Ceramid is frequently con-
108 sidered the central hub of sphingolipid metabolism, and is converted to higher-order
109 sphingolipids (including sphingosine, sphingomyelin, and galactosylceramide) within the
110 Golgi and at the plasma membrane (Holthuis & Menon, 2014). These species are further
111 modified via phosphorylation, glycosylation, and sulfidation to produce a dynamic popu-
112 lation of dozens of distinct lipid species in constant flux (Gault, Obeid, & Hannun, 2010).
113 The sphingolipid synthesis pathway, and the resulting proportions of its products, can be
114 manipulated using an array of genetic and chemical tools.

115 The chemical inhibitor myriocin (Myr) blocks the activity of the SPT complex, pre-
116 venting the synthesis of all lipid species with the sphingoid base; similarly, the inhibitor

117 Fumonisin B1 (FB1) blocks ceramide synthase activity to produce a defect in the synthe-
118 sis of all high order sphingolipids. We confirmed the potency of these inhibitors in three
119 phagocytosis-competent cell lines through radioactive labeling with 3-L-(^{14}C)-serine. Total
120 lipids were extracted and analyzed using thin layer chromatography (TLC) and autoradi-
121 ography. For THP-1 and U937 human monocyte-derived macrophages, RAW 264.7 mu-
122 rine macrophages, and DC2.4 murine dendritic cells, three-day treatment with Myr and
123 FB1 (at 15uM and 5uM, respectively) resulted in significantly reduced levels of (^{14}C)-
124 sphingomyelin – demonstrating the capacity of these drugs to block sphingolipid synthe-
125 sis (Fig. 1A and B, and data not shown).

126 To orthogonally investigate the effects of chemical inhibition of sphingolipid syn-
127 thesis, we prepared genetic knockouts of Sptlc2 (one of the two primary SPT complex
128 members) in RAW 264.7 and DC2.4 cells using CRISPR/Cas9 genomic editing. We ver-
129 ified knockdown using Western blotting (Fig1C), and then assessed the capacity of these
130 cells to synthesize sphingolipids using TLC and autoradiography (Fig. 1D+E). To further
131 characterize of the effects of Sptlc2 knockout, we performed lipidomics analysis of RAW
132 264.7 macrophages using liquid chromatography coupled with tandem mass spectrome-
133 try. We found all observed sphingolipid species to be depleted in Sptlc2-/- cells relative
134 to wildtype levels, whereas other lipid species were unaffected (Fig. 1F).

135 Finally, to characterize the effects of myriocin and FB1 treatment, as well as Sptlc2
136 knockout, on cell survival and growth, we performed proliferation and survival assays. We
137 found that there was no significant difference in morphology, proliferation, or survival
138 (Supp. Fig. 1 and data not shown). We subsequently found that RAW 264.7 Sptlc2-/- cells

139 display normal membrane trafficking through in pulse-chase assessment of [^{35}S]-methio-
140 nine/cysteine incorporation and protein secretion (Supp. Fig. 1B).
141
142 *Sphingolipid depletion results in impaired phagocytic uptake of* M.tb
143 To investigate the role of sphingolipids during phagocytic uptake of *M.tb*, we used
144 Myr and FB1 to block sphingolipid synthesis in THP-1, RAW 264.7, and DC2.4 cells, in-
145 fected with an mCherry-expressing strain *of M.tb,* and quantified treated versus untreated
146 cells. Briefly, cells were infected at a multiplicity of infection (MOI) of 10 for two hours,
147 after which cells were fixed and stained with 1) Alexa Fluor 488-conjugated phalloidin to
148 visualize F-actin at cell boundary and 2) DAPI to visualize nuclei for cell count. Fluores-
149 cence microscopy was used to quantify uptake efficiency. Efficiency was calculated
150 through automated counting of cell number (by nuclei) and internalized bacteria (red flu-
151 orescent particles within green cell boundary).We report uptake efficiency as the ratio of
152 total number of internalized *M.tb* particles against the number of identified nuclei, and
153 normalized the uptake rate of treated cells to that of untreated cells. Both THP-1 and
154 U937 monocyte-derived macrophages treated with Myr or FB1 showed a significant im-
155 pairment in phagocytosis compared to untreated cells, with a reduction in uptake of [60
156 and 40% respectively] (Fig. 2A-D). RAW 264.7 macrophages and DC 2.4 dendritic cells
157 both displayed similar reductions in phagocytic uptake following Myr and FB1 treatment
158 with decreases of 80% (Fig. 2E-H).
159 We next assessed the capacity of Sptlc2-/- RAW 264.7 and DC 2.4 cells to inter-
160 nalize *M.tb* using a similar paradigm: two-hour infection with mCherry-expressing *M.tb*,
161 followed by fixation and staining with Alexa Fluor 488-conjugated phalloidin and DAPI.

162 Fluorescence microscopy was performed and analyzed as above. In agreement with our
163 previous results, we find that in both RAW 264.7 and DC 2.4 cells, Sptlc2 knockout results
164 in a significant decrease in *M.tb* uptake compared to wildtype (Fig. 2 I-L). Together with
165 the results of chemical inhibition, these results suggest that the maintenance of total cel-
166 lular sphingolipid levels through sphingolipid synthesis is required for efficient uptake of
167 *M.tb* across all of our model cell lines.
168
169 *Sphingolipid depleted cells recognize and bind pathogen-particles, but are defective in*
170 *proper phagosome formation*
171 Phagocytosis is strictly regulated through a signaling network that involves the dy-
172 namic activation and recruitment of both enzymes (such as GTPases, kinases, and phos-
173 phatases) and lipids – particularly several phosphatidylinositol species. As a target parti-
174 cle is engaged at the cell membrane, the aggregation of ligand-bound phagocytic receptor
175 initiates a sequence of phosphorylation that activates the Rho GTPases RAC1 and
176 Cdc45, which subsequently activate phosphatidylinositol 5-kinase. This kinase catalyzes
177 a localized increase in phosphatidylinositol 4,5-*bis*phosphate ($PI_{(4,5)}P_2$). High $PI_{(4,5)}P_2$ lev-
178 els initiate actin assembly at the base of the nascent phagosome, driving the membrane
179 into a leading edge that works around the target particle. As this leading edge progresses
180 away from the base of the nascent phagosome, local $PI_{(4,5)}P_2$ levels at the base are re-
181 duced via three mechanisms. First, it may be converted through phosphorylation by phos-
182 phatidylinositol 3-kinase (PI_3K) to form phosphatidylinositol 3,4,5-*tris*phosphate
183 ($PI_{(3,4,5)}P_3$),which initiates actin disassembly and recycling at the trailing edge. In parallel,
184 $PI_{(4,5)}P_2$ is degraded by phosopholipase C-gamma (PLCγ) into the secondary messengers

185 diacylglycerol (DAG) and inositol 1,4,5-trisphosphate (IP_3), which activate innate immune
186 response components such as NFκB. Finally, $PI_{(4,5)}P_2$ is also degraded to $PI_{(4)}P$ by phos-
187 phatases OCRL and INPP5B. Evidence suggests that the trailing wave of $PI_{(4,5)}P_2$ degra-
188 dation following phagosome assembly is critical for the complete phagocytic uptake of a
189 target particle (Levin et al., 2015). To date, however, there have been no reports connect-
190 ing phosphoinositide signaling and sphingolipids during phagocytosis.

191 To assess the roles played by sphingolipids during this signaling cascade, we chal-
192 lenged wildtype and Sptlc2-knockout RAW 264.7 cells with Alexa594-conjugated zymo-
193 san A particles. Zymosan A is an inert bead composed of fungal β-glucan that is engaged
194 by phagocytic receptors to stimulate particle engulfment in macrophages and dendritic
195 cells (Underhill, 2003). Using fluorescence microscopy and several transfected fusion
196 protein biosensors, we quantified the spatiotemporal enrichment of activated GTPases
197 Rac1 and Cdc42, $PI_{(4,5)}P_2$, $PI_{(3,4,5)}P_3$, and F-actin at the phagocytic cup (Schlam et al.,
198 2015).

199 First, wildtype and Sptlc2-deficient RAW 264.7 macrophages were transfected
200 with PAK(PBD)-YFP – this fusion construct binds activated Rac1/Cdc42 GTPases
201 through the p21-binding domain of the Protein Activated Kinase (Hoppe & Swanson,
202 2004; Schlam et al., 2015; Srinivasan et al., 2003). Cells were then challenged with zy-
203 mosan A and the localization of the reporter construct was quantified through live-cell
204 fluorescence imaging. Phagocytic uptake was partitioned into five stages (*Start*, *Recog-*
205 *nition*, *Engulfment*, *Internalization*, and *End*) and the localized enrichments of biosensor
206 in at least four cells were quantified for each stage. We show that both wildtype and
207 Spltc2-deficient cells display an increase in Rac1/Cdc42 activity at the pseudopod after

208 binding zymosan A particles (Fig. 3A). As the wildtype cells fully engulf particles, there is
209 a concomitant increase in YFP signal intensity, followed by a sharp decline in YFP signal
210 at the phagosome as the bead is fully internalized and Rac1/Cdc42 activity is terminated.
211 In contrast, over the span of imaging, Sptlc2-deficient cells fail to fully engulf or internalize
212 particles, and correspondingly, there is a defect in the aggregation of YFP signal. By
213 quantifying the degree of enrichment at each stage, we observe a marked overall reduc-
214 tion in the spatiotemporal activity of the Rac1 and Cdc42 GTPases in the Sptlc2 knockout
215 cells. (Fig. 3B).

216 To characterize subsequent stages of the phagocytic signaling cascade, we visu-
217 alized the dynamics of $PI_{(4,5)}P_2$ at the phagosome using the PH(PLCδ)-GFP reporter con-
218 struct (Schlam et al., 2015) – which binds to $PI_{(4,5)}P_2$ through the PH domain of phospho-
219 lipase-C *delta*. As above, wildtype and Sptlc2-deficient RAW 264.7 macrophages were
220 transfected with the reporter construct, challenged with zymosan A, and visualized using
221 fluorescence live-cell imaging. As with the local increases of Rac1 and Cdc42 activity at
222 the pseudopod, both the wildtype and the Sptlc2 knockout cells display an enrichment of
223 $PI_{(4,5)}P_2$ upon particle recognition. However, $PI_{(4,5)}P_2$ enrichment peaks as wildtype cells
224 begin engulfing particles, whereas Sptlc2-deficient cells never reach a significant enrich-
225 ment of reporter signal at the nascent phagosome and again fail to internalize the particles
226 (Fig. 3C). Quantification again shows a statistically significant gap in $PI_{(4,5)}P_2$ aggregation
227 at the phagosomal cup, further suggesting an impairment of phagocytic signaling follow-
228 ing particle recognition (Fig. 3D).

229 Next, we visualized $PI_{(3,4,5)}P_3$ at the site of particle engagement of wildtype and
230 Sptlc2 knockout RAW 264.7 macrophages by transfection with the PH(AKT)-GFP fluo-
231 rescent biosensor. This reporter construct is composed of the PH domain of the protein
232 kinase Akt and GFP (Marshall et al., 2001). As this phosphatidylinositol species is re-
233 quired for actin disassembly at the trailing edge of pseudopod progression, we also used
234 the F-actin biosensor LifeAct to visualize actin dynamics in the developing phagosome.
235 Unlike with Rac1/Cdc42 activity and $PI_{(4,5)}P_2$ localized concentration, Sptlc2 knockout
236 cells never attain the degree of $PI_{(3,4,5)}P_3$ enrichment that wildtype cells quickly reach upon
237 particle recognition (Fig. 3E and F). Accordingly, imaging with LifeAct demonstrates that
238 F-actin cycling is aberrant in Sptlc2 knockout cells (Fig. 3G and H).
239 Together, these data suggest that sphingolipids play a critical role in the proper
240 maturation of the phagosome, but are dispensable components of the early stages of
241 particle binding and recognition.
242
243 *Perturbation of sphingomyelin levels at exoplasmic leaflet inhibits* M.tb *uptake*
244 Because sphingomyelin is particularly enriched to the outer leaflet of the plasma
245 membrane, we hoped to investigate the role that this specific lipid species plays during
246 the phagocytic uptake of *M.tb*. First, to determine the local enrichment of sphingomyelin
247 at the phagocytic synapse, we briefly infected THP-1 macrophages with zymosan A par-
248 ticles, and stained sphingomyelin at the exoplasmic leaflet using purified GFP-lysenin.
249 The protein lysenin is a pore-forming toxin derived from the earthworm *Eisenia foetida*
250 and binds specifically to sphingomyelin – and GFP-conjugated lysenin, purified from bac-

251 terial expression, serves as a functional staining tool for visualizing localized concentra-
252 tions of sphingomyelin (Kinoshita et al., 2017; Yamaji et al., 1998). We find that after 10
253 minutes of exposure to zymosan, sphingomyelin is enriched at the phagocytic cup upon
254 receptor binding (data not shown). These data corroborate prior findings that sphingomy-
255 elin is enriched to domains such as lipid rafts and caveolae, and suggest that this specific
256 sphingolipid species plays an important role in efficient phagocytosis (Kinoshita, Suzuki,
257 Murata, & Matsumori, 2018).

258 To further characterize the role of sphingomyelin at the cell surface during *M.tb*
259 infection, we endeavored to manipulate the levels of sphingomyelin at the cell surface
260 and quantify uptake through fluorescence microscopy. Sphingomyelin is synthesized
261 along the secretory pathway by sphingomyelin synthase 1 (Sgms1), and within lysosomal
262 compartments by Sgms2. We isolated clonal knockouts of the Sgms1 gene in U937
263 monocytes using CRISPR/Cas-9 genomic editing. As above, we infected these and
264 wildtype cells for 2 hours and quantified uptake through fluorescence microscopy. We
265 found that Sgms1-deficient cells are impaired in their capacity to internalize *M.tb* to a
266 similar degree as cells depleted of all sphingolipids (Fig. 4A and B). Thus, we conclude
267 that sphingomyelin plays a significant role in the phagocytic uptake of *M.tb*, and that this
268 lipid species contributes significantly to our observed results on the effect of total sphin-
269 golipid depletion reported above. Further efforts to characterize the effects of sphingomy-
270 elin-specific depletion are ongoing.

271

272 **Discussion**

273 In this study, we report that the capacity of *M.tb* to invade host cells by engagement
274 of phagocytic receptors is significantly dependent on the presence of host sphingolipids
275 at the cell membrane. This result corroborates our prior observations on the uptake of
276 *Candida albicans* (Tafesse et al., 2015). In that publication, we demonstrated that sphin-
277 golipid depletion inhibits the phagocytic clearance of this fungal pathogen, and that sphin-
278 golipid-depleted mice are more susceptible to death by infection due to systemic candid-
279 iasis. The observations we report here similarly agree with prior reports that sphingolipids
280 – particularly ceramide – are required for defense against infection by *Pseudomonas ae-*
281 *ruginosa.* This process occurs through the formation of sphingolipid-enriched membrane
282 platforms on epithelial cells that enable the clustering of receptors that mediate innate
283 immune response to pathogens (Grassmé et al., 2003).

284 Using a total of four human and murine phagocytic cell models (THP-1, U937,
285 RAW 264.7, and DC 2.4), we demonstrate that chemical and genetic tools may be used
286 to deplete total levels of bulk sphingolipids, and that these sphingolipid-deficient phago-
287 cytes are incapable of taking up *Mycobacterium tuberculosis.* This phenotype is mirrored
288 in the genetic blockade of sphingomyelin synthesis at the cell surface via CRISPR/Cas9
289 deletion of Sphingomyelin synthase-1 in U937 human monocytes. These results demon-
290 strate the importance of sphingolipids in the context of this cellular process. However, it
291 is notable that sphingolipid depletion does not totally ablate phagocytic uptake.

292 There are several possible explanations to this observation. First, the sphingolipid
293 salvage pathway of these cells remains intact – any sphingolipids in the growth medium
294 may be taken up to a degree that provides cells with sufficient quantities of sphingolipids

295 to eventually phagocytose *M.tb* particles, despite a reduction in total efficiency. Alterna-
296 tively, the limited rate of uptake we observe may be due to limitations in visualization and
297 quantification; bacteria which may appear to be internalized may in fact not actually be
298 fully within the host cell. In particular, we note that there is overlap between bacterial
299 fluorescent signal and plasma membrane in approximately 50% of U937 Sgms1-/- cells,
300 whereas this is the case for only 20% of bacteria in control cells (data not shown). The
301 incorporation of an antibiotic treatment during infection may clarify this possibility. In
302 agreement with this possibility, Hauck and colleagues have used treatment of ectopic
303 acid sphingomyelinase enzyme to deplete cells of sphingomyelin at the exoplasmic leaflet
304 to show that the internalization of N. gonorrhoeae was reduced, but that its binding to the
305 cell surface was not affected (Hauck et al., 2000).

306 In addition to the initial observations of defective internalization of *M.tb* by sphin-
307 golipid-deficient hosts, we present a possible mechanism through which sphingolipids
308 enable the propagation of phagocytic signaling by coordinating the dynamics of phospho-
309 inositide turnover. Upon engagement of phagocytic receptor to cognate ligand, Rho
310 GTPases Rac1 and Cdc42 are activated and initiate the localized production of $PI_{(4,5)}P_2$.
311 This local increase in the concentration of $PI_{(4,5)}P_2$ initiates F-actin polymerization at the
312 base of the forming phagocytic cup, which drives pseudopodia around the particle. Con-
313 comitantly, the proper progression of the pseudopod (and the subsequent full engulfment
314 of the particle) necessitates F-actin disassembly and recycling; this process is driven by
315 the conversion of $PI_{(4,5)}P_2$ to $PI_{(3,4,5)}P_3$ via PI3K (Schlam et al., 2015). Because we observe
316 defects in the propagation of this signaling pathway upon depletion of sphingolipids, we
317 believe that sphingolipids, sphingomyelin in particular, are responsible for coordinating

318 the necessary interactions between kinases and phosphoinositide substrates. One can-
319 didate of interest for further investigation is PI3K, which may require interaction or mem-
320 brane tethering with one or more sphingolipids at the site of phagocytic receptor engage-
321 ment..

322 This study represents, to our knowledge, the first evidence for sphingolipids as
323 regulators of phosphoinositide turnover during phagocytosis. However, prior work has
324 shown that sphingolipids play roles in phosphoinositide signaling in other contexts. For
325 example, phosphatidylinositol 4-phosphate (PI_4P) has been implicated in the transfer of
326 ceramides from the ER to the Golgi by interacting with the ceramide transfer protein CERT
327 (Hanada et al., 2003). Additionally, Capasso and colleagues showed that sphingomyelin
328 production triggers dephosphorylation of PI_4P at the trans-Golgi as a negative feedback
329 mechanism, suggesting regulatory interplay that maintains cellular levels of sphingomy-
330 elin (Capasso et al., 2017).

331 Collectively, this study demonstrates that sphingolipids are indispensable for the
332 phagocytosis of *Mycobacterium tuberculosis*. In the context of infection with this patho-
333 gen, phagocytosis represents a double-edged sword. As phagocytosis represents the in-
334 vasive mechanism of entry for this pathogen, it may be of interest to investigate mecha-
335 nisms of inhibiting the interactions between host phagocytes and *M.tb.* However, phago-
336 cytosis also represents a significant mechanism through which professional antigen pre-
337 senting cells activate and hone the adaptive immune response – without the capacity to
338 efficiently sense and probe the internal environment, host organisms may be at greater
339 risk of death by systemic infection, as was observed in the context of *C. albicans* (Tafesse
340 et al., 2015). Despite this conundrum, it is essential to understand the mechanisms

through which pathogens harness host factors to initiate infection. This study represents an important step in understanding the mechanisms of pathogenesis in *Mycobacterium tuberculosis* infection; we hope that such work contributes to the development of new therapeutic strategies to fight this ancient pathogen.

Materials and Methods

Reagents. Myriocin and Fumonisin B1 were purchased from Cayman Chemical Company. 3-L-[14C]serine with a specific activity of ??? was purchased from ???. Phorbol 12-myristate 13-acetate (PMA) was purchased from Abcam?. 4% Paraformaldehyde was from Fisher Scientific. Alexa Fluor® 488 Phalloidin and Zymosan A (S. cerevisiae) BioParticles Alexa Fluor 594 conjugate were purchased from Thermo Fisher. Rabbit polyclonal antibody against phospho-PI3 Kinase p85 (Tyr458)/p55 (Tyr199) (p-PI3K) (#4228) was purchased from Cell Signaling Technology. Mouse Monoclonal antibody against GAPDH (ab8245) was purchased from Abcam. Anti-rabbit IgG, HRP-linked antibody and anti-mouse IgG, HRP-linked antibody were purchased from Cell Signaling.

Plasmids

Active (GTP-bound) Rac1/Cdc42 was detected with PAK(PBD)-YFP, a plasmid encoding the PBD of PAK fused to YFP (Hoppe 2004.). $PI(_{4,5})P_2$ was detected with PH(PLCδ)-GFP, a plasmid encoding the PH domain of PLCδ fused to GFP (kindly provided by Grinstein). $PI(_{3,4,5})P_3$ levels were monitored by PH(AKT)-GFP, a plasmid encoding the PH domain of AKT fused to GFP (Feng 2014). F-actin was monitored by LifeAct-GFP, a F-actin staining peptide fused to GFP (Riedl 2008).

362 The plasmids used for generation of lentivirus consists of the pCDH-CMV(-)-sgRNA plas-
363 mid, the psPAX2 plasmid (packaging) and pMD2.G plasmid (envelope). pCW-Cas9 len-
364 tivirus was kindly provided by David Sabatini (Whitehead Insititute for Biomedical Re-
365 search)

366 **Cell culture and drug treatment**

367 THP-1, U937, Raw 264.7 and DC 2.4 cells were routinely cultured in RPMI medium sup-
368 plemented with 10% FBS (Seradigm) and 1% Pen Strep (Gibco). HeLa cells were cul-
369 tured in DMEM supplemented with 10% FBS and 1% Pen Strep. All cell lines were cul-
370 tured at 37 °C and 5% CO_2.

371 THP-1 and U937 cells were differentiated to macrophages by 50ng/ml PMA for 1 day in
372 RPMI medium supplemented with 10% FBS, after which the cells were treated with 5μM
373 myriocin or fumonisin B1 for 3 days in RPMI supplemented with 10% FBS and 1%PS.

374 **Radio-active labeling and TLC**

375 $500x10^3$ THP-1, U937, and RAW cells were seeded into a well of a 6-well plate, differen-
376 tiated and treated as described above (Cell culture and drug treatment). After 3 days of
377 drug treatment the cells were labeled with 2μCi/ml ??? of 3-L-[^{14}C]-serine for 4 hours in
378 Opti-MEM supplemented with the appropriate drug concentration of myriocin and FB1
379 and incubated at 37°C. Cells were washed two times with PBS and lipid extraction was
380 done following Bligh and Dyer method (Bligh and Dyer 1959). The methanol/chloroform-
381 lipid extracts were dried by nitrogen gas. Dried lipids were re-dissolved in a few drops of
382 chloroform/methanol (1:2, vol/vol) and loaded on a TLC plate. Lipids were separated by
383 developing the TLC plate first in acetone and then in a mixture of chloroform, methanol

384 and 25% ammonia solution (50:25:6, vol/vol/vol). Radiolabeled lipids were detected on a
385 Phosphor-Imager (Company?).

386 **Generation of Lentivirus. (Fikadu)**

387 Doxycycline inducible Cas9 expressing plasmid, pCW-Cas9, was kindly provided by Da-
388 vid Sabatini (Whitehead Institute for Biomedical Research). Lentivirus was produced by
389 co-transfection of HEK 293T cells with the pCDH-sgRNA/pCW-Cas9 and psPAX2 and
390 pMD2.G. Transfection was performed with Lipofectamine 3000 (Thermo Fisher) accord-
391 ing to manufacturer's instructions. Cells were cultured in DMEM supplemented with
392 10%FBS and the growth medium was replaced after 6 hours. 48 hours after transfection,
393 lentivirus-containing supernatant was harvested, centrifuge for 5mins at 1250 rpm and
394 filtered through a 0.45μm filter.

395 **Generation of stable Raw264.7 inducible Cas9 cell lines.**

396 Raw264.7 cells were infected with lentivirus (pCW-Cas9) encoding Cas9 cDNA, and were
397 cultured in media containing 7 μg/mL of puromycin (Sigma Aldrich).

398 **Generation of CRISPR/Cas9-mediated Sptlc2-/- Raw264.7 cell line. (Fikadu)**

399 Potential target sequences for CRISPR interference were found with the rules outlined in
400 (Mali 2013). The following seed sequences (CRISPR target sequences) preceding the
401 PAM motif that were found in the exon of Sptlc2 gene were used: Sptlc2 #1 GAAC-
402 GGCTGCGTCAAGAAC; Sptlc2 #2: AGCAGCACCGCCACCGTCG Potential off-target
403 effects of the seed sequence were confirmed using the NCBI Mus musculus Nucleotide
404 BLAST. Generation of CRISPR/Cas9-mediated Sptlc2-knockout Raw264.7 cell line was
405 performed as described in (Tafesse 2014). Briefly, CRISPR gBlock was designed to clone

406 into the restriction enzymatic site NheI/BamHI of pCDH-CMV(-) (SBI; CD515B-1) as fol-
407 lows: cacagtcagacagtgactcaGTGTCACAgctagcTTTCCCATGATTCCTTCATATTT-
408 GCATA-
409 TACGATACAAGGCTGTTAGAGAGATAATTAGAATTAATTTGACTGTAAACACAAAGA
410 TATTAGTACAAAATACGTGACGTAGAAAGTAATAATTTCTTGGGTAGTTTGCAG-
411 TTTTAAAATTATGTTTTAAAATGGACTATCATATGCTTACCGTAACTTGAAAGTATTT
412 CGATTTCTTGGCTTTATATATCTTGTGGAAAGGACGAAACAC-
413 CGnnnnnnnnnnnnnnnnn-
414 nGTTTTAGAGCTAGAAATAGCAAGTTAAAATAAGGCTAGTCCGTTATCAACTTGAAA
415 AAGTGGCACCGAGTCGGTGCTTTTTTTggatccTGTGCACAgtcagtcacagtcagtctac (n:
416 CRISPR target sequences). The gBlock was then digested using the restriction enzymes
417 NheI and BamHI and ligated into pCDH-CMV(-) vector that was linearized by digesting
418 with the same restriction enzyme.
419 The Cas9-inducible cells were infected with lentivirus carrying pCDH-CMV(-)-sgRNA, and
420 were cultured in media containing 250 µg/mL of hygromycin B (Life Technology). To in-
421 duce expression of Cas9, cells were treated with 2 µg/mL of doxycycline (Clontech) for
422 3–5 days. Clonal selection was performed by single cell dilution on 96-well plates. The
423 individual colonies were collected and the expression of Sptlc2 was examined by western-
424 blotting using Sptlc2 antibody. Or TLC?
425 **U937 SGMS1 -/- cell lines**
426 U937 SGSM1 -/- cells were kindly provided by Sebastian Virreira Winter (Max Plack Insi-
427 tute) and the CRISPR/Cas9-mediated knock out cell lines were established as described
428 in Winter et al., 2016 (Winter 2016).

429 **Culturing of *Mycobacterium tuberculosis***

430 Culturing and infection of *Mycobacterium tuberculosis (M.tb)* was conducted in a Bi-
431 osafety-level 3 laboratory following general safety guidelines. *M.tb* strain H37R, express-
432 ing constitutively mCherry, was cultured at 37°C in 7H9 Broth medium supplemented with
433 50µg/ml hygromycin B.

434 **Infection of macrophages with *M.tb***

435 For infection of THP-1 and U937 cells, the cells were seeded into a SensoPlate™ 96-
436 Well Glass-Bottom Plates (Greiner Bio-One) at a density of $15x10^3$ cells per well in RPMI
437 supplemented with 10% FBS, 1% PS and 50ng/ml PMA at 37°C. 1 day after differentiation
438 THP-1 cells were treated for 3 days with 5µM myriocin or fumonisin B1. Infection with
439 *M.tb* was performed after 3 days of differentiation of U937 cells and 3 days of drug treat-
440 ment of differentiated THP-1 cells. THP-1 and U937 cells were infected with a multiplicity
441 of infection (MOI) of 50 in RPMI supplemented with 10% FBS for 4 hours at 37°C.

442 For infection of Raw264.7 and DC2.4 cells, $20x10^3$ cells / well were seeded 24 hours prior
443 infection into a SensoPlate™ 96-Well Glass-Bottom Plates (Greiner Bio-One) and cul-
444 tured in RPMI 10%FBS, 1%PS at 37°C. Raw264.7 and DC2.4 cells were infected with a
445 MOI of 10 in RPMI supplemented with 10% FBS for 4 hours at 37°C.

446 After 4 hours *M.tb* containing supernatant was aspirated and cells were washed one time
447 with PBS and then fixed with 4% PFA over night at 4°C.

448 **Microscopy**

449 Spinning disk confocal (SDC) imaging was performed on a Yokogawa CSU-W1 SDC
450 microscope (Nikon, Tokyo, Japan) using a 20x Plan Apo VC (NA 0.75) objective and a
451 60x Plan Apo VC (NA 1.4) oil immersion objective equipped with a Andor's Zyla sCMOS

452 camera under the control of the Nikon acquisition software and a stage motorized in
453 X,Y. Live cell imaging was performed at 37°C and 5% CO_2 using a multi-position imag-
454 ing with an automated focusing at each time point. Representative images were ana-
455 lyzed and prepared using the FIJI software.
456 Further quantitative imaging was performed on a Keyence BZ-X700 all in one fluores-
457 cence microscope (Keyence Corporation, Osaka, Japan) using a 40x Plan Apo oil im-
458 mersion objective, and controlled using the Keyence BZ-X Viewer software. Image anal-
459 ysis was performed using Keyence BZ-X Analyzer software and FIJI.
460 **Phagocytosis assay**
461 Fixed cells were washed twice with PBS and incubated in PBS for 15 min in Permaebili-
462 zation Buffer (0.1% Triton X-100 and 1%BSA). Cells were stained with Phalloidin-Alexa
463 488 (Thermo Fisher) at a final concentration of 33nM for 60 min and washed one time
464 with PBS. After the Phalloidin-staining, cells were stained with 1xDAPI for 10 mins and
465 washed 3 times with PBS. THP-1 cells were then imaged using the SDC microscope
466 (Nikon) with a 20x objective and the U937, Raw264.7 and DC2.4 cells were imaged with
467 the Keyence BZ-X700 with a 20x objective. The parameters for imaging were kept the
468 same for each sample. For image analysis either the Nikon or Keyence BZ-X Analyzer
469 software was used. In brief: The outline of the cells was determined via the A488 signal
470 (Phalloidin-staining) and the number and area of mCherry (*M.tb*) signal in the A488 sig-
471 nal was detected by the program. In a second round the number of cells was deter-
472 mined by counting the nuclei via the DAPI staining. Number of bacteria / area of
473 mCherry-signal inside the cell was divided by the number of cells analyzed to identify
474 the phagocytosis efficiency.

475 **Live imaging of phagocytosis**

476 For transient transfection, Raw264.7 cells were seeded into a SensoPlate™ 96-Well
477 Glass-Bottom Plates at a cell number of $10x10^3$ cells/well 24 hours prior transfection.
478 Transfection was conducted with Lipofectamine 3000 (Thermo Fisher) according to
479 manufacturer's instructions. Briefly, 100ng of plasmid DNA and 0.2µl of P3000 reagent
480 were mixed in 5µl Opti-MEM and 0.33µl Lipofectamine 3000 was mixed in 5µl Opti-
481 MEM. Both reagent dilutions were mixed together and allowed to sit for 15 min. The mix
482 was then added directly to the appropriate well and mixed by swirling the plate gently.
483 For the imaging, the growth medium was aspirated and replaced with RPMI without
484 phenol red containing Zymosan A Bioparticles A595 (Thermo Fisher) at an MOI of 20.
485 The 96-well plate were centrifuged at 1000rpm for 1 mins. The cells were imaged with
486 the SDC microscope (Nikon) and 3-4 different spots per well were imaged at the same
487 time for 60 min with capture intervals of 15 sec. The parameters for imaging were kept
488 the same for each sample.

489 **Live imaging analysis**

490 Out of all cells imaged, those which showed to recognize a zymosan particle and main-
491 tained a heathy phenotype throughout the whole imaging process were selected for fur-
492 ther analysis. Imaging analysis was performed using FIJI software (Schindelin et al.,).
493 The parameters for image processing were kept constant when comparing different
494 data sets. The area of the phagosome was selected, cropped and opened in a new win-
495 dow. For the original image, the threshold was set automatically on the GFP-channel
496 and for the threshold of the GFP-phagosome area, the threshold of the whole cell was
497 multiplied by 1.5 to ensure that only an increase in signal is counted (GFP-threshold cell

498 x 1.5 = GFP-threshold phagosome area). The threshold area at different time points
499 was measured by the analyze-measure function of FIJI and the results were exported
500 into Excel (Microsoft). The values for the GFP-threshold of the phagosome area were
501 divided by the values for the GFP-threshold of the whole cell at the corresponding time
502 points.

503 **Immunoblotting**

504 Differentiated THP-1 cells treated with myriocin or left untreated were infected with *M.tb*
505 at a MOI of 20 for 10 and 20 mins or left uninfected. And, differentiated U937 WT and
506 SGSM1 -/- cells were infected with *M.tb* at a MOI of 20 for 5 and 10 mins or left uninfected.
507 Afterwards, the washed cells were lysed and post-nuclear fractions were subjected to
508 12% SDS-PAGE and separated by electrophoresis, before being transferred to methanol-
509 activated Polyvinylidene difluoride membranes. Membranes were blocked in Tris-buff-
510 ered saline (TBS) supplemented with 0.1% Tween 20 (TBS-T) and 5% bovine serum
511 albumin (BSA) for 30 min. Primary antibodies against p-PI3K and GAPDH were used in
512 3% BSA TBS-T at 1:1000 dilutions and incubated over night or 60 min, respectively. HRP-
513 conjugated antibodies were used at a 1:5000 dilution with an incubation time of 60 min.
514 Membranes exposed to ECL western blotting substrate (GE Life Science) were visualized
515 using the ImageQuant LAS 4000. Brightness/Contrast were adjusted globally across the
516 entire image using the FIJI software. Immunoblots were cropped for presentation; see
517 Supplementary Fig. 5 for uncropped images.

518

519

520

521 **References**

522 Cambier, C. J., Falkow, S., & Ramakrishnan, L. (2014). Host evasion and exploitation
523 schemes of Mycobacterium tuberculosis. *Cell*, *159*(7), 1497–1509.
524 https://doi.org/10.1016/j.cell.2014.11.024

525 Daniel, T. M. (2006). The history of tuberculosis. *Respiratory Medicine*, *100*(11), 1862–
526 1870. https://doi.org/10.1016/j.rmed.2006.08.006

527 El Alwani, M., Wu, B. X., Obeid, L. M., & Hannun, Y. A. (2006). Bioactive sphingolipids
528 in the modulation of the inflammatory response. *Pharmacology and Therapeutics*,
529 *112*(1), 171–183. https://doi.org/10.1016/j.pharmthera.2006.04.004

530 García-Arribas, A. B., Alonso, A., & Goñi, F. M. (2016). Cholesterol interactions with
531 ceramide and sphingomyelin. *Chemistry and Physics of Lipids*, *199*, 26–34.
532 https://doi.org/10.1016/j.chemphyslip.2016.04.002

533 Gault, C., Obeid, L., & Hannun, Y. (2010). An overview of sphingolipid metabolism: from
534 synthesis to breakdown Introduction to Sphingolipid Metabolism. *Adv Exp Med Biol*,
535 *688*, 1–23. https://doi.org/10.1007/978-1-4419-6741-1_1

536 *Global tuberculosis report 2018.* (2018). Geneva.

537 Grassmé, H., Jendrossek, V., Riehle, A., von Kürthy, G., Berger, J., Schwarz, H., …
538 Gulbins, E. (2003). Host defense against Pseudomonas aeruginosa requires
539 ceramide-rich membrane rafts. *Nature Medicine*, *9*, 322. Retrieved from
540 https://doi.org/10.1038/nm823

541 Hakomori, S. I., & Igarashi, Y. (1995). Functional role of glycosphingolipids in cell
542 recognition and signaling. *Journal of Biochemistry*, *118*(6), 1091–1103.
543 https://doi.org/10.1093/oxfordjournals.jbchem.a124992

544 Hannun, Y. A., & Obeid, L. M. (2002). The ceramide-centric universe of lipid-mediated
545 cell regulation: Stress encounters of the lipid kind. *Journal of Biological Chemistry*,
546 *277*(29), 25847–25850. https://doi.org/10.1074/jbc.R200008200
547 Hla, T., & Dannenberg, A. J. (2012). Sphingolipid Signaling in Metabolic Disorders. *Cell*
548 *Metabolism*, *16*(4), 420–434. https://doi.org/10.1016/j.cmet.2012.06.017
549 Holthuis, J. C. M., & Menon, A. K. (2014). Lipid landscapes and pipelines in membrane
550 homeostasis. *Nature*, *510*(7503), 48–57. https://doi.org/10.1038/nature13474
551 Hoppe, A. D., & Swanson, J. A. (2004). Cdc42, Rac1, and Rac2 Display Distinct
552 Patterns of Activation during Phagocytosis. *Molecular Biology of the Cell*, *15*(8),
553 3509–3519. https://doi.org/10.1091/mbc.e03-11-0847
554 Kinoshita, M., Suzuki, K. G. N., Matsumori, N., Takada, M., Ano, H., Morigaki, K., …
555 Murata, M. (2017). Raft-based sphingomyelin interactions revealed by new
556 fluorescent sphingomyelin analogs. *Journal of Cell Biology*, *216*(4), 1183–1204.
557 https://doi.org/10.1083/jcb.201607086
558 Kinoshita, M., Suzuki, K. G. N., Murata, M., & Matsumori, N. (2018). Evidence of lipid
559 rafts based on the partition and dynamic behavior of sphingomyelins. *Chemistry*
560 *and Physics of Lipids*, *215*(May), 84–95.
561 https://doi.org/10.1016/j.chemphyslip.2018.07.002
562 Levin, R., Grinstein, S., & Schlam, D. (2015). Phosphoinositides in phagocytosis and
563 macropinocytosis. *Biochimica et Biophysica Acta (BBA) - Molecular and Cell*
564 *Biology of Lipids*, *1851*(6), 805–823. https://doi.org/10.1016/j.bbalip.2014.09.005
565 Malik, Z. A., Thompson, C. R., Hashimi, S., Porter, B., Iyer, S. S., & Kusner, D. J.
566 (2003). Cutting Edge: Mycobacterium tuberculosis Blocks Ca2+ Signaling and

567 Phagosome Maturation in Human Macrophages Via Specific Inhibition of
568 Sphingosine Kinase. *The Journal of Immunology*, *170*(6), 2811–2815.
569 https://doi.org/10.4049/jimmunol.170.6.2811
570 Marshall, J. G., Booth, J. W., Stambolic, V., Mak, T., Balla, T., Schreiber, A. D., …
571 Grinstein, S. (2001). Restricted accumulation of phosphatidylinositol 3-kinase
572 products in a plasmalemmal subdomain during Fcγ receptor-mediated
573 phagocytosis. *Journal of Cell Biology*, *153*(7), 1369–1380.
574 https://doi.org/10.1083/jcb.153.7.1369
575 Schlam, D., Bagshaw, R. D., Freeman, S. A., Collins, R. F., Pawson, T., Fairn, G. D., &
576 Grinstein, S. (2015). Phosphoinositide 3-kinase enables phagocytosis of large
577 particles by terminating actin assembly through Rac/Cdc42 GTPase-activating
578 proteins. *Nature Communications*, *6*(1), 8623. https://doi.org/10.1038/ncomms9623
579 Snider, A. J., Alexa Orr Gandy, K., & Obeid, L. M. (2010). Sphingosine kinase: Role in
580 regulation of bioactive sphingolipid mediators in inflammation. *Biochimie*, *92*(6),
581 707–715. https://doi.org/10.1016/j.biochi.2010.02.008
582 Srinivasan, S., Wang, F., Glavas, S., Ott, A., Hofmann, F., Aktories, K., … Bourne, H. R.
583 (2003). Rac and Cdc42 play distinct roles in regulating PI(3,4,5)P3 and polarity
584 during neutrophil chemotaxis. *Journal of Cell Biology*, *160*(3), 375–385.
585 https://doi.org/10.1083/jcb.200208179
586 Stuart, L. M., & Ezekowitz, R. A. B. (2005). Phagocytosis : Elegant Complexity Review,
587 *22*, 539–550. https://doi.org/10.1016/j.immuni.2005.05.002
588 Tafesse, F. G., Rashidfarrokhi, A., Schmidt, F. I., Freinkman, E., Dougan, S., Dougan,
589 M., … Ploegh, H. L. (2015). Disruption of Sphingolipid Biosynthesis Blocks

590 Phagocytosis of Candida albicans. *PLoS Pathogens*, *11*(10), 1–27.
591 https://doi.org/10.1371/journal.ppat.1005188
592 Taha, T. A., Mullen, T. D., & Obeid, L. M. (2006). A house divided: Ceramide,
593 sphingosine, and sphingosine-1-phosphate in programmed cell death. *Biochimica*
594 *et Biophysica Acta - Biomembranes*, *1758*(12), 2027–2036.
595 https://doi.org/10.1016/j.bbamem.2006.10.018
596 Thompson, C. R., Iyer, S. S., Melrose, N., VanOosten, R., Johnson, K., Pitson, S. M., …
597 Kusner, D. J. (2005). Sphingosine Kinase 1 (SK1) Is Recruited to Nascent
598 Phagosomes in Human Macrophages: Inhibition of SK1 Translocation by
599 Mycobacterium tuberculosis. *The Journal of Immunology*, *174*(6), 3551–3561.
600 https://doi.org/10.4049/jimmunol.174.6.3551
601 Underhill, D. M. (2003). Macrophage recognition of zymosan particles. *Journal of*
602 *Endotoxin Research*, *9*(3), 176–180. https://doi.org/10.1179/096805103125001586
603 van Meer, G., & de Kroon, A. I. P. M. (2011). Lipid map of the mammalian cell. *Journal*
604 *of Cell Science*, *124*(1), 5–8. https://doi.org/10.1242/jcs.071233
605 Yamaji, A., Sekizawa, Y., Emoto, K., Sakuraba, H., Inoue, K., Kobayashi, H., & Umeda,
606 M. (1998). Lysenin, a novel sphingomyelin-specific binding protein. *The Journal of*
607 *Biological Chemistry*, *273*(9), 5300–5306. Retrieved from
608 http://www.ncbi.nlm.nih.gov/pubmed/9478988
609
610

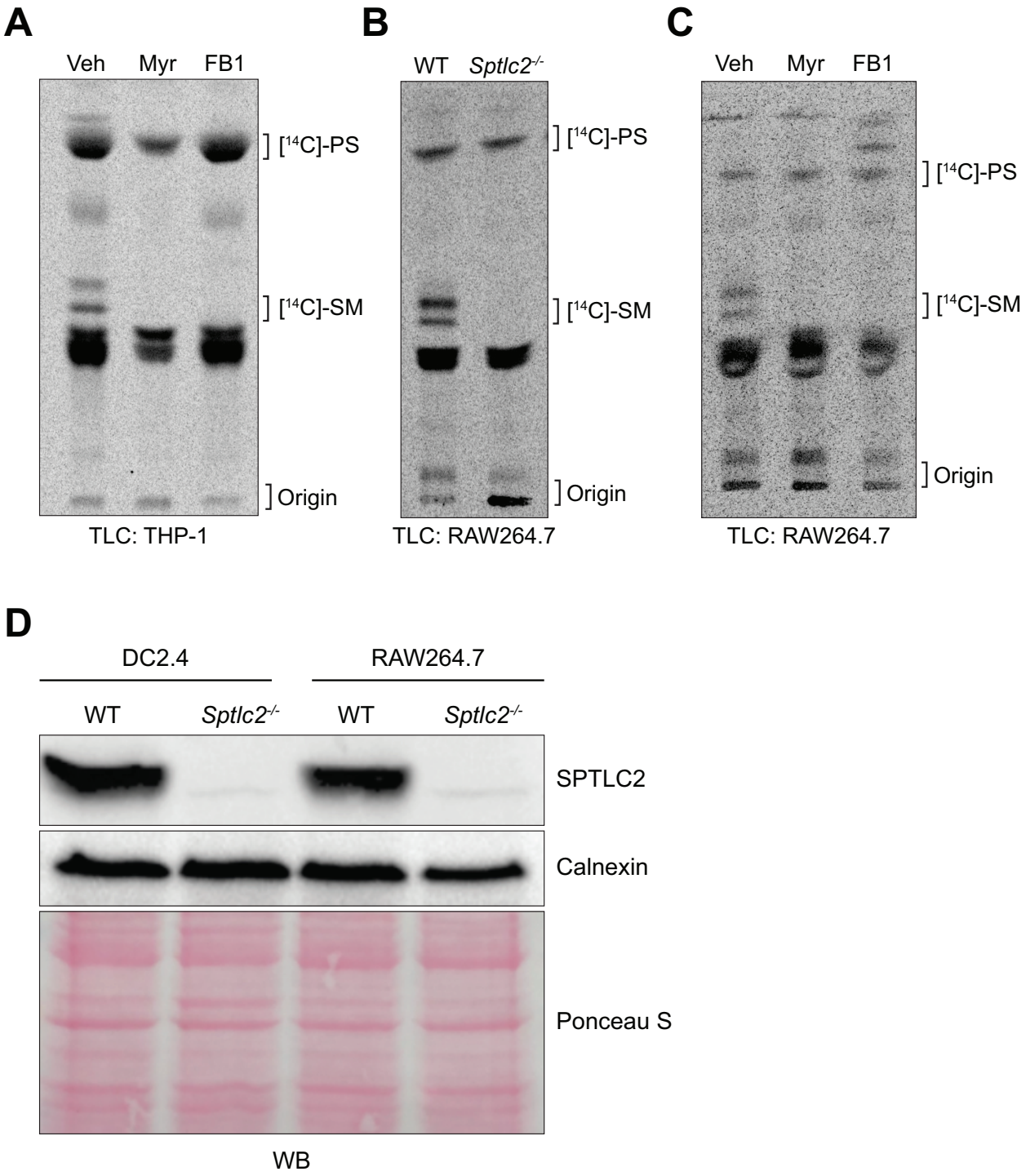

611

612 Figure 1.

613

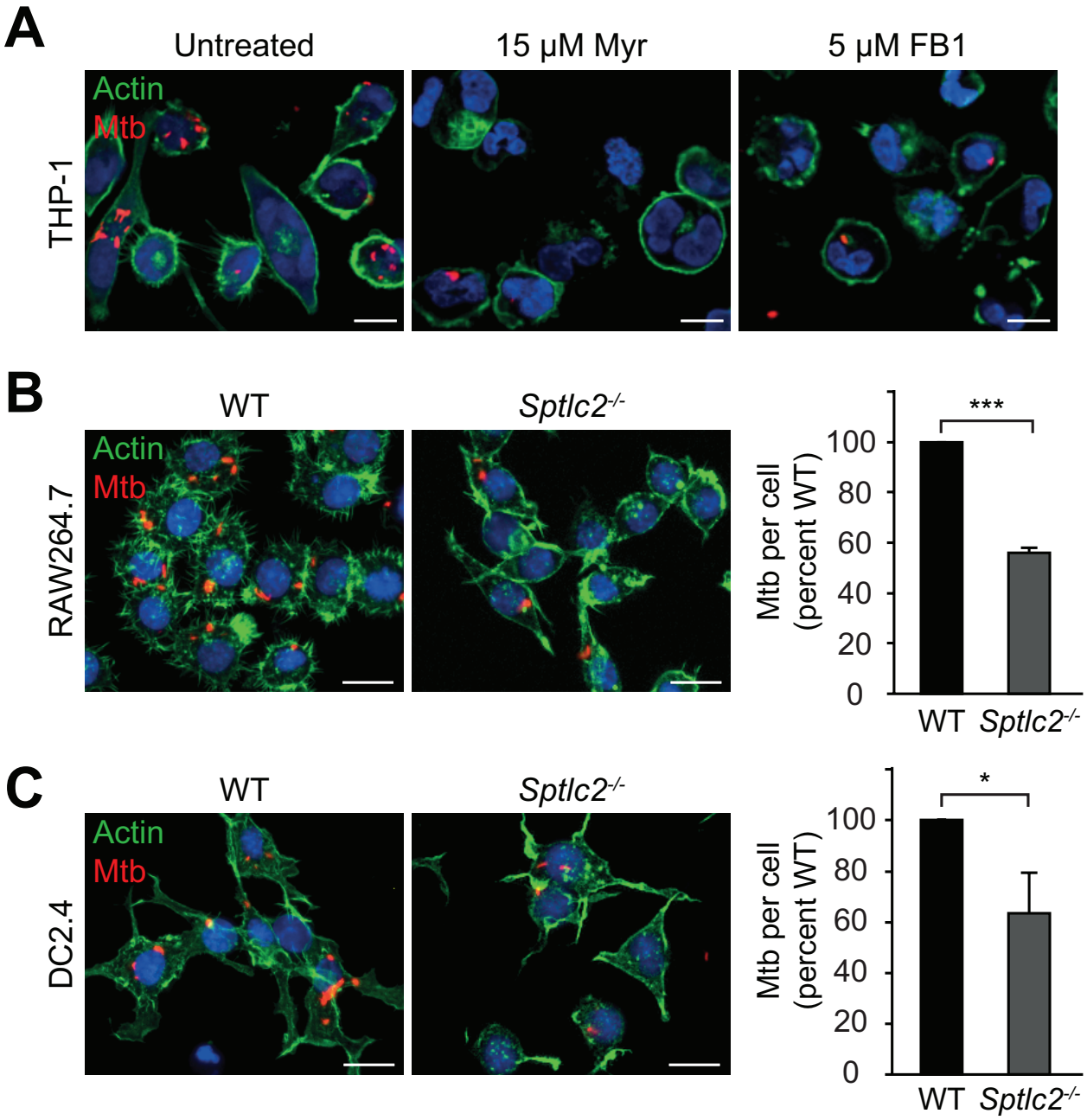

614

615 Figure 2.